Evidence of a ZnCr$_2$Se$_4$ Spinel Inclusion at the Core of a Cr-Doped ZnSe Quantum Dot

Weiwei Zheng,[†] Kedar Singh,[†,‡] Zhenxing Wang,[†] Joshua T. Wright,[§] Johan van Tol,[†,‖] Naresh S. Dalal,[†,‖] Robert W. Meulenberg,[§] and Geoffrey F. Strouse*,[†]

[†]Department of Chemistry and Biochemistry, Florida State University, Tallahassee, Florida 32306, United States

[‡]Department of Physics, Banaras Hindu University, Varanasi, 221005, India

[§]Laboratory for Surface Science and Technology and Department of Physics and Astronomy, University of Maine, Orono, Maine 04469, United States

[‖]National High Magnetic Field Laboratory, Tallahassee, Florida 32310, United States

S *Supporting Information*

ABSTRACT: Herein we report doping of ZnSe by Cr ions leads to formation of small ZnCr$_2$Se$_4$ spinel inclusions within the cubic sphalerite lattice of a 2.8 nm CrZnSe quantum dot (QD). The Cr ion incorporates as a pair of Cr(III) ions occupying edge-sharing tetragonal distorted octahedral sites generated by formation of three Zn ion vacancies in the sphalerite lattice in order to charge compensate the QD. The site is analogous to the formation of a subunit of the ZnCr$_2$Se$_4$ spinel phase known to form as inclusions during peritectoid crystal growth in the ternary CrZnSe solid-state compound. The oxidation state and site symmetry of the Cr ion is confirmed by X-ray absorption near edge spectroscopy (XANES), crystal field absorption spectroscopy, and electron paramagnetic resonance (EPR). Incorporation as the Cr(III) oxidation state is consistent with the thermodynamic preference for Cr to occupy an octahedral site within a II−VI semiconductor lattice with a half-filled t$_{2g}$ d-level. The measured crystal field splitting energy for the CrZnSe QD is 2.08 eV (2.07 eV form XANES), consistent with a spinel inclusion. Further evidence of a spinel inclusion is provided by analysis of the magnetic data, where antiferromagnetic (AFM) exchange, a Curie−Weiss (C−W) temperature of $\theta = -125$ K, and a nearest-neighbor exchange coupling constant of $J_{NN} = -12.5$ K are observed. The formation of stable spinel inclusions in a QD has not been previously reported.
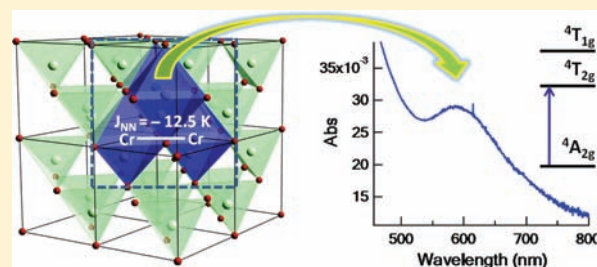
INTRODUCTION

The ability to incorporate paramagnetic ions into a semiconductor quantum dot (QD) lattice is of great interest to the solid-state materials community due to the ability to couple s−p−d orbital exchange-induced magnetic properties with the size-dependent QD energy levels.[1,2] The excitement of incorporating a magnetic ion into an otherwise nonmagnetic host lattice reflects the potential of such materials for quantum computing, spintronics, magneto-resistive, and magneto-optical applications.[3] While chemists are intrigued by the ability to control the location and concentration of the dopant ions as a crystallite grows,[4−9] physicists are interested in the novel spin properties that arise[10−12] and the influence of QD surfaces.[13−15] For years it was considered nearly impossible to consistently dope a II−VI lyothermally grown QD due to self-annealing effects.[1,3] Over the past several years the realization that a single source cluster precursor can be used to generate a predoped nucleus has led to the opportunity to efficiently incorporate a range of dopant ions into the whole II−VI series.[3,7] In II−VI semiconductors, incorporation of a dopant metal ion with the same charge (i.e., Mn(II), Cr(II), and Co(II)) leads to simple substitutional incorporation of the ion

of interest up to its solubility limit.[16−18] Incorporation of an ion that has a different charge, such Cu(I) or Eu(III), results in formation of ion vacancies in the QD in order to reach charge neutrality.[19,20]

One magnetic dopant ion that has received little attention in the QD community is chromium. In Cr-doped II−VI semiconductors, the incorporation of Cr(I),[21,22] Cr(II),[23,24] and Cr(III)[25,26] have been reported by solid-state synthesis. Of the three oxidation states, the Cr(III) oxidation state is preferred due to its one-half-filled t$_{2g}$ level and has been shown to be naturally introduced into octahedral (O_h) sites formed by ion vacancies that charge compensate the lattice in the otherwise tetrahedral coordination environment observed in II−VI semiconductors (ZnS, ZnSe, CdS, CdSe).[27] Synthesis of the Cr(III)-doped II−VI semiconductor occurs via a peritectoid decomposition reaction leading to formation of a AB$_2$X$_4$ spinel structure by the group II metal occupying the tetrahedral (T_d) site (A site) and the Cr(III) ion occupying the O_h site (B site).[28] The spinel phase is a singularity in the phase

diagram and does form as a precipitated inclusion due to its low solubility in the II−VI lattice over a wide range of Cr to metal ion ratios.[29] Cr(III) incorporation leads to formation of a spinel phase that exhibits a complex interplay between the charge, lattice, and spin degrees of freedom, with reported ferromagnetic (FM) states observed in $CdCr_2Se_4$ and a helical spin state in $ZnCr_2Se_4$.[30−32] The complex magnetism in spinels of II−VI semiconductors have been reported to exhibit large magnetoresitivity and multiferrocity, demonstrating their potential for magneto-optics.[33−35] Although these structures are reported in bulk, few reports have appeared for Cr doping at the nanoscale.[18]

In this manuscript, we report to the best of our knowledge the first study on Cr(III) incorporation into ZnSe QDs. The incorporation of chromium into a 2.8 nm ZnSe QD occurs as Cr(III) ions occupying a tetragonal distorted O_h site within the cubic ZnSe lattice, as evidenced by X-ray absorption near edge spectroscopy (XANES) and optical absorption crystal field analysis. The structural inclusion of the Cr(III) center is believed to form $ZnCr_2Se_4$ unit cells precipitated within the ZnSe QD by forming six localized Zn ion vacancies opening four O_h holes for the Cr(III) ion. Such a formation is stable within the cubic structure and observed in bulk systems.[36] The MCr_2Se_4 (M = Hg, Cd, Zn) spinel structural motif as an inclusion has only been investigated in the bulk phase and in thin films to date.[37] Analogous to the reported results herein, vacancy formation in a QD to accommodate O_h site occupation for Eu(III) in CdSe QDs has been observed by XANES and extended X-ray absorption fine structure (EXAFS) analysis in previous publications.[20] The ability of the QD to incorporate a defect that can be lattice matched to the QD is similar to the reported formation of nanocrystal inclusions via endotaxial growth in bulk crystal of $AgPb_mSbTe_{2+m}$.[38]

Evidence for the proposed spinel precipitated inclusions of the form $ZnCr_2Se_4$ is observed in the magnetic experimental data where competitive antiferromagnetic−ferromagnetic (AFM−FM) exchange with an exchange coupling constant (J_{NN} = −12.5 K) is observed, which is consistent with $ZnCr_2Se_4$. The formation of a spinel precipitate in the ZnSe QD zinc blende lattice is intriguing and offers a new class of dilute magnetic semiconductor QDs to be explored. It is believed the spinel formation reflects a thermodynamic process due to the more favorable coordination and electronic state for a Cr(III) d^3 transition metal as an O_h coordinated species with a half-filled t_{2g} level. Further studies are underway to determine the magneto-optical physics and exchange coupling between the $ZnCr_2Se_4$ inclusion and the host lattice band levels. The initial study opens the opportunity to explore the rich magneto-optical physics of the Cr(III) spinel phase incorporated as a precipitated inclusion within QDs and may suggest isolation of a single phase spinel QD can be achieved under appropriate reaction conditions.

■ EXPERIMENTAL SECTION

Chemicals. Hexadecylamine (HDA) (90%, Acros Organics), $CrCl_2$ (99.9%, Acros Organics), toluene (>99.9%, EMD Chemicals), and methanol (MeOH, >99.8%, VWR) were used as supplied. $Li_4[Zn_{10}Se_4(SePh)_{16}]$ cluster was prepared similar as described previously.[39]

Synthesis of Cr(III)-Doped ZnSe DMSQDs. The synthesis of 0, 0.4, 1.0, 2.5, and 4.0 mol % Cr(III)-doped ZnSe QDs was performed under N_2 using a previously reported single source precursor method employing the reaction of a $Li_4[Zn_{10}Se_4(SePh)_{16}]$ cluster with $CrCl_2$ at a concentration of 0, 2, 5, 10, and 20 mol % Cr to Zn. Briefly, the QDs

are prepared by the dissolution of 500 mg (0.15 mmol) of $Li_4[Zn_{10}Se_4(SePh)_{16}]$ cluster and $CrCl_2$ in ∼40 mL of HDA at 100 °C under N_2. The reaction mixture was heated to 220 °C (10 °C/min) for 6 h, inducing QD growth.[39−41] Isolation of $Zn_{1−x}Cr_xSe$ QDs from the reaction mixture is achieved by standard precipitation methods carried out under N_2 to prevent surface oxidation. The precipitation protocol requires the addition of a minimal amount of toluene to dissolve the reaction mixture at 60 °C followed by dropwise addition of methanol to induce nanocrystal aggregation and precipitation. The precipitate is collected via centrifugation and redissolved in toluene. The process is repeated three times to ensure reagent-free particles. The samples are isolated and maintained under N_2 in a drybox to prevent formation of ZnO.

The Cr, Zn, and Se content was determined by using an Oxford Instruments ED2000 X-ray fluorescence (XRF) spectrometer with a Cu K_α source. Based upon XRF analysis, the isolated $Zn_{1−x}Cr_xSe$ QD samples contain 0, 0.4, 1.0, 2.5, and 4.0 mol % Cr by carrying out the reactions at 0, 2, 5, 10, and 20 mol % Cr. For a standard XRF measurement, the powdered QD samples were completely dissolved in 90% HNO_3, heated to remove excess NO_x, and then diluted to ∼3 mL with a 2% HNO_3 solution to allow compatibility with the XRF sample holder.

QD Characterization. The isolated $Zn_{1−x}Cr_xSe$ QD size, dispersity, morphology, and structure were analyzed by transmission electron microscopy (TEM) and TEM-selected area electron diffraction (TEM-SAED) using a JEOL-2010 microscope operated at 200 kV. The size dispersity is analyzed for over 100 QDs. The SAED map for the QDs was assigned to lattice planes based upon the observed d-spacing. The QDs were dispersed on holey carbon (400 mesh) from a toluene solution.

The size of the QD measured by TEM was verified by analysis of the first exciton transition ($1S_{3/2} \rightarrow 1S_e$) for ZnSe in the optical absorption spectroscopy.[39] The room temperature optical absorption spectra were measured on toluene solutions of the $Zn_{1−x}Cr_xSe$ QDs at ∼$10^{−6}$ M concentrations in a 1 cm quartz cuvette using a Varian Cary 50 UV−vis spectrophotometer.

Ensemble structural characterization of the isolated QDs is performed using a powder X-ray diffractometer (pXRD). The pXRD patterns were recorded on about 10 mg samples on a Rigaku DMAX 300 Ultima III pXRD using Cu K_α (λ = 1.5418 Å). QD sizing by Scherer analysis of the (111), (220), and (311) reflection in pXRD provides validation of the optical and TEM size analysis and more importantly provides further support for the high crystallinity of the samples.[39]

High-frequency electron paramagnetic resonance (HF-EPR) measurements over 100−406.4 GHz at 10 K were made for the 2.5% $Zn_{1−x}Cr_xSe$ QDs. The HF-EPR measurements were conducted at the Florida State University National High Magnetic Field Laboratory (FSU-NHMFL) in Tallahassee, FL. The HF-EPR operates in transmission mode and employs oversized cylindrical waveguides, as described elsewhere.[42−44] Microwave detection was performed with a low-noise, fast-response InSb hot-electron bolometer (QMC Ltd.). For the EPR experiments, the samples were dried powders.

Assignment of the Cr Oxidation State and Site Symmetry. Assignment of the oxidation state and the site of occupation (T_d vs O_h holes) for the Cr ion in the ZnSe QD was accomplished by analysis of the Cr $L_{2,3}$ edge by soft XANES spectroscopy between 570 to 600 eV for the 2.5% $Zn_{1−x}Cr_xSe$. XANES measurements were acquired at the spherical grating monochromator beamline at the Canadian Light Source at the University of Saskatchewan.[45] The QD samples were dissolved in toluene, allowed to slowly evaporate on a Si wafer, mounted onto carbon tape, and introduced into an ultrahigh vacuum chamber (P ∼ low $10^{−8}$ to low $10^{−9}$ Torr). XANES experiments were conducted using the total electron yield method, where the total photocurrent into the sample is measured as the photon energy is scanned through the absorption edge. The current from a highly transmissive gold grid was used to normalize the XANES spectra. Crystal field absorption spectra of solution samples by UV−vis on all doping concentrations confirm Cr oxidation state and site symmetry.
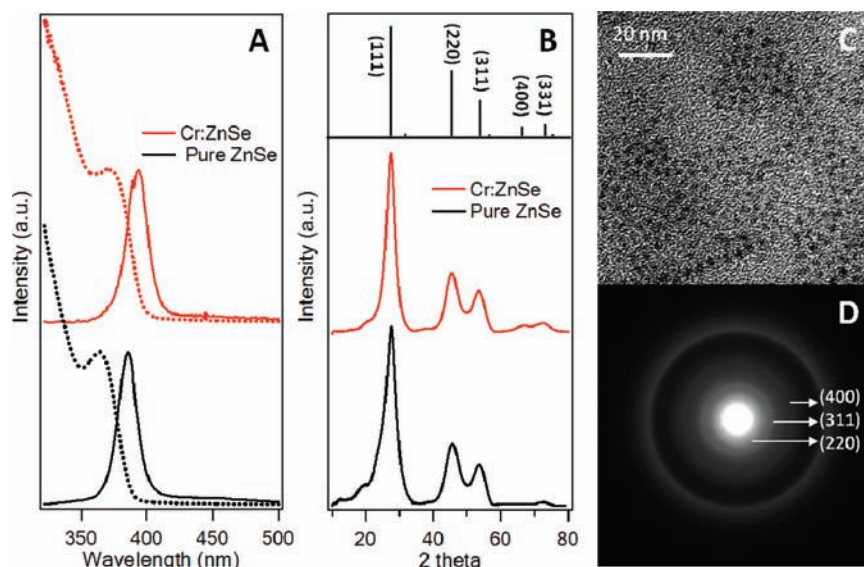
Figure 1. Characterization data for 2.8 ± 0.1 nm 2.5% $Zn_{1-x}Cr_xSe$ QDs. (A) Absorption (dashed) and photoluminescence (solid) spectra for ZnSe and 2.5% $Zn_{1-x}Cr_xSe$ QDs. (B) pXRD patterns for ZnSe and 2.5% $Zn_{1-x}Cr_xSe$ QDs relative to the standard ZnSe card (01-070-0777, $F\bar{4}3m$ (216)). (C) TEM image for 2.5% $Zn_{1-x}Cr_xSe$ QD at 600 000 magnification (scale bar 20 nm). (D) TEM-SAED image for 2.5% $Zn_{1-x}Cr_xSe$ QDs measured over 2000 nm^2.

Magnetic Characterization. The magnetic properties of the 2.5% $Zn_{1-x}Cr_xSe$ QDs were measured on powdered samples using a Quantum Design MPMS XL7 superconducting quantum interference device magnetometer (SQUID). Zero-field cooled (ZFC) and field cooled (FC, 0.02 T) susceptibility measurements were collected for dc-susceptibility over the range of 2−300 K. Field-dependent magnetization (M) was measured between −7 to +7 T.

■ RESULTS AND DISCUSSION

Using the single source cluster synthetic method, spherical Cr(III)-doped ZnSe QDs were isolated from a lyothermal reaction with ~5% size dispersity based on TEM analysis (Figure 1 and Figure SF1, Supporting Information). X-ray fluorescence analysis (XRF) allow the isolated QDs to be described as $Zn_{1-x}Cr_xSe$ solid solution with x = 0.000, 0.004, 0.010, 0.025, and 0.040 (0.0, 0.4, 1.0, 2.5, and 4.0%). The optical absorption data (Figure 1A and Figure SF2, Supporting Information) for the $Zn_{1-x}Cr_xSe$ QD samples exhibit a well-defined $1S_{3/2} \rightarrow 1S_e$ excitonic feature for all doping levels. Analysis of the optical absorption of the first exciton[39] ($1S_{3/2} \rightarrow 1S_e$, Figure SF2, Supporting Information) and TEM (Figure SF1, Supporting Information) yields QD sizes of 2.4 nm for 0.0%, 2.6 nm for 0.4%, 2.6 nm for 1.0%, 2.8 nm for 2.5%, and 2.7 nm for 4.0%. The energy of the first absorption feature for all $Zn_{1-x}Cr_xSe$ samples is consistent with the measured TEM QD size, indicating well-formed QDs are obtained from the reaction process. Based on XRF analysis, the Cr ion incorporation occurs at ~20% of the reaction stoichiometry, reflecting the solubility of the Cr precursor in the reaction conditions, the differences in the Zn and Cr precursor activity, and the rate of ion addition onto the growing QD. The mole ratio of cation to anion in the isolated QD is nearly constant across the doping concentration range (Table 1, Supporting Information), reflecting the experimental uncertainty in XRF for estimating lattice vacancy formation. The photoluminescence (PL) data for the $Zn_{1-x}Cr_xSe$ samples in Figure 1A exhibits Gaussian profiles for all samples with a peak full width at half-maximum (fwhm) = 18 ± 1 nm. The PL is assignable to ZnSe bandgap emission with no discernible feature for the Cr

center at room temperature between 300 and 700 nm (Figure SF2A, Supporting Information). The PL intensity for the ZnSe bandgap PL is dependent on the Cr ion concentration. A plot of the ZnSe PL quantum yield vs Cr concentration shows a decrease in PL intensity with increasing Cr content (Figure SF2B, Supporting Information). The loss of intensity of the ZnSe PL with increasing Cr content can be understood in terms of nonradiative decay to a low-lying crystal field level centered on the Cr center. Dopant-dependent quenching has been observed in ion-doped QDs previously.[8]

Selected pXRD data for $Zn_{1-x}Cr_xSe$ (0.0% and 2.5%) is shown in Figure 1B. In addition, the pXRD data for the 4.0% QDs are shown in Figure SF3, Supporting Information. The powder pattern for the samples exhibits identical profiles that can be indexed to the spahlerite (zinc blende) $F\bar{4}3m$ structure. The assignment of the zinc-blende phase is confirmed by inspection of the d-spacing for the (220), (331), and (400) reflections in the TEM-SAED pattern collected over a ~2000 nm^2 area for 2.5% $Zn_{1-x}Cr_xSe$ (Figure 1D). No concentration-dependent shift in the (111), (220), or (311) pXRD reflection can be observed within experimental error. No pXRD or SAED reflections can be identified for Cr_2Se_3 or $ZnCr_2Se_4$ impurity phases (Figure SF3, Supporting Information).

Oxidation State and Subtituional Site of the Cr Dopant. It is well established the Cr ion can incorporate into ZnSe with variable oxidation states. The oxidation state of the Cr in the $Zn_{1-x}Cr_xSe$ QD was analyzed by XANES spectroscopy of the Cr $L_{2,3}$ edge. The XANES data in Figure 2Ai for the 2.5% $Zn_{1-x}Cr_xSe$ sample shows two discrete features, a broad L_3 edge absorption feature at ~578 eV with a shoulder to higher energy, and a weaker L_2 edge absorption at ~586 eV. The energy and spectral shape of the $L_{2,3}$ edge in the 2.5% $Zn_{1-x}Cr_xSe$ QD sample (Figure 2Ai) allow definitive assignment of the Cr oxidation state as Cr(III) based on comparison to simulated $L_{2,3}$ edge XANES spectra.[46]

The substituional site for the Cr ion in the ZnSe lattice can be analyzed by comparison to the calculated spectra for a theoretical $Zn_{1-x}Cr_xSe$ sample in which Cr(II) (Figure 2Bi),
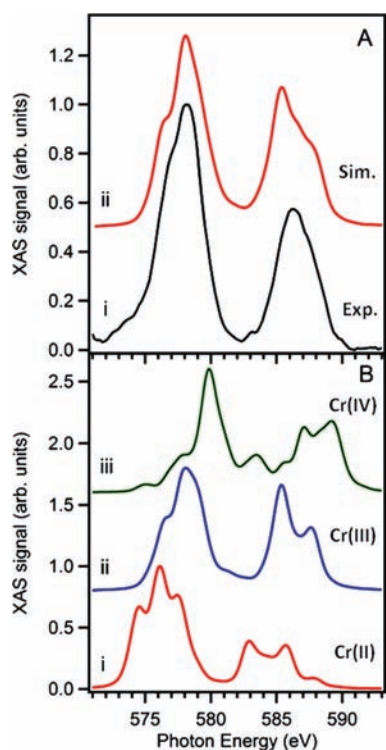
Figure 2. Cr $L_{2,3}$ edge X-ray absorption spectra. (A) (i) 2.5% $Zn_{1-x}Cr_xSe$ QDs and (ii) simulated tetragonally distorted O_h crystal field (2.07 eV) for Cr(III). (B) XANES simulation of Cr ions in a perfect O_h field (10 Dq = 2.07 eV): (i) Cr(II), (ii) Cr(III), and (iii) Cr(IV).

Cr(III) (Figure 2Bii), and Cr(IV) (Figure 2Biii) occupy an O_h coordination site with a crystal field energy of 10 Dq = 2.07 eV, as shown in Figure 2B. The theoretically calculated spectrum for Cr(III) in an O_h field fits the energy of the observed $L_{2,3}$ edge but does not reproduce the shape of the spectra. The experimental XANES data for the 2.5% $Zn_{1-x}Cr_xSe$ QD (Figure 2Ai) compared to the calculated spectra show the observed broadening of the L_2 edge is not well reproduced by the perfect O_h site simulation. A better fit to the experimental XANES data is obtained by inducing a tetragonal distortion of the site with a crystal field of 10 D_q = 2.07 eV (Figure 2Aii). The crystal field terms from XANES, which include the terms D_s and D_t, suggest compression occurs along the z-axis for the Cr(III)—Se bond. The tetragonal distortion is not surprising, as removal of three Zn ions for every two Cr(III) ions produces an incorporation site in which the Cr(III) ion can be bound as two edge-sharing O_h that would be tetragonally distorted if the lattice does not relax about the vacancy. Similar observations of the formation of a distorted six-coordinate site by Cd ion vacancy formation to allow charge balance were made for Eu(III) incorporation into CdSe by XANES and EXAFS analysis.[20]

The coordination of the Cr(III) center by six Se ions can be proven by measurement of the crystal field spectra. An approximate O_h coordination site for Cr(III) will produce a set of d–d absorption features observable in the visible centered at ~560 nm ($^4A_{2g} \rightarrow {}^4T_{2g}$) and a second absorption feature centered at ~440 nm for the $^4A_{2g} \rightarrow {}^4T_{1g}$ transition.[47,48] Tetragonal distortion will reduce the symmetry, resulting in splitting of the T_{2g} and T_{1g} levels, which is typically observed as a broadening of the $^4A_{2g} \rightarrow {}^4T_{2g}$ transition. The concentration-dependent crystal field optical absorption spectra for the

$Zn_{1-x}Cr_xSe$ QD samples is shown in Figure 3. By multipeak fitting of the absorption data the energy of the $^4A_{2g} \rightarrow {}^4T_{2g}$
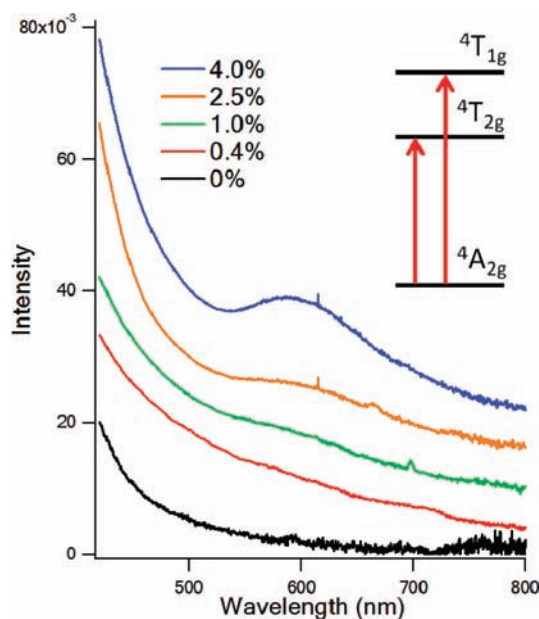

Figure 3. Absorption spectra (298 K) in concentrated toluene solution for 0, 0.4, 1.0, 2.5, and 4.0 $Zn_{1-x}Cr_xSe$ QDs. Insert shows the allowed crystal field transitions of Cr(III) ion in an O_h crystal field.

crystal field transition can be extracted from the exciton tail observed in Figure 3, allowing assignment of the $^4A_{2g} \rightarrow {}^4T_{2g}$ transition at 595 nm (2.08 eV) (Figure SF4, Supporting Information). The feature exhibits a clear concentration dependence, confirming the assignment. The transition is broadened as anticipated by the lowered symmetry observed in the XANES data. The energy of the $^4A_{2g} \rightarrow {}^4T_{2g}$ Cr(III) crystal field transition is equivalent to the crystal field energy, allowing a value of 10 Dq = 2.08 eV to be directly measured. The value of 10 Dq is consistent with the calculated XANES value of 2.07 eV. The higher lying crystal field transitions for the $^4A_{2g} \rightarrow {}^4T_{1g}$, which lies at approximately 440 nm, is obscured due to overlap with the first exciton transition in the ZnSe QD and cannot be assigned, therefore the Racah parameters cannot be extracted from the experimental data. The crystal field spectroscopy results support the assignment of Cr(III) occupying a tetragonally distorted six-coordinate site within the ZnSe lattice.

Further evidence of Cr(III) (d³, S = 3/2) can be confirmed from high-frequency EPR (HF-EPR) data. For Cr(III) in the O_h crystal field, the $^4A_{2g}$ orbital singlet is responsible for the observed EPR absorption. The EPR spectrum of the isotopes of Cr(III) without nuclear spin can be described by the Zeeman term only, since the zero-field splitting would be negligible in a strict octahedral symmetry (Figure SF5, Supporting Information). The EPR spectrum will consist of a single peak with a Landé g-value of slightly less than 2.00, due to spin–orbit coupling. Hyperfine contributions will not be observed in the powder spectra since the ^{53}Cr isotope is only 9.55% abundant; each hyperfine structure line has an intensity of approximately 1/42 of that of the main peak.[49] The frequency-dependent EPR spectra for the 2.8 nm 2.5% $Zn_{1-x}Cr_xSe$ QD sample measured at 100, 112, 200, 216, 304.8, 324, and 406.4 GHz (10 K) are shown in Figure 4A. The observation of the single sharp
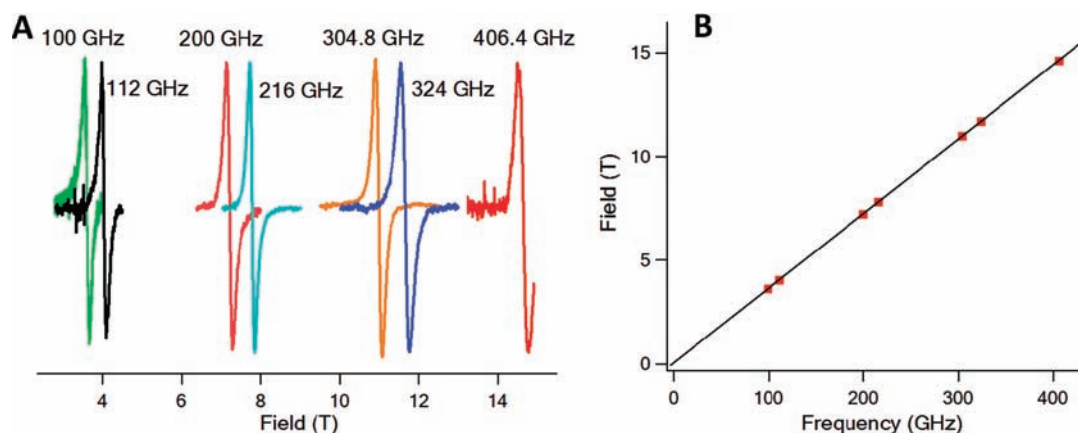
Figure 4. (A) Frequency-dependent EPR measurements at 10 K for 2.5% $Zn_{1-x}Cr_xSe$ QD. (B) Frequency-dependent on EPR central resonance field of 2.5% $Zn_{1-x}Cr_xSe$ QD. The slope yields a g-value of 1.9808.

resonance over all frequencies is consistent with a Cr(III) ion (d^3, $S = 3/2$) since the zero-field splitting for Cr(III) is typically small.[50]

An accurate value of the Landé g-value for the Cr(III) center in the $Zn_{1-x}Cr_xSe$ QD can be obtained by plotting the frequency dependence of the center field (Figure 4B). The plot yields a g-value of 1.9808 consistent with the prediction for a Cr(III) ion coordinated by six Se ions.[51,50] The deviation of the g-value from the spin only value of $g_e = 2.0023$ is caused by a contribution from triplet T_2 to the orbital moment of the ground state. The observed EPR pattern and g-value are not consistent with assignment of Cr(II) or Cr(I).[23,50] Experimentally observed g-values are 1.9985 for Cr(II)[52] and 2.0018 for Cr(I).[53] Furthermore, the zero-field splitting of Cr(II) ion (d^4, $S = 2$) is usually larger than 2 cm^{-1} with a negative sign, which would result in the appearance of multiple transitions in the EPR spectra (M_s: $-2 \rightarrow -1$, $-1 \rightarrow 0$, $0 \rightarrow +1$, and $+1 \rightarrow +2$ transitions),[23,50] which are not observed in Figure 4.

$ZnCr_2Se_4$ Spinel Inclusion formation. Since the structural data from TEM and pXRD are in good agreement, the results strongly imply a high degree of crystallinity exists for the CrZnSe QD, which in effect implies that the Cr(III) ions incorporate with minimal lattice distortion. The spectroscopy results confirm the Cr ion is incorporated into the ZnSe lattice as a Cr(III) ion occurring at a tetragonally distorted six-coordinate site in an otherwise sphalerite lattice for the Zn and Se sublattices. Addition of one Cr(III) must induce removal of one and a half Zn(II) centers to balance the QD charge, if the Cr(III) ion incorporates into the core of the QD. More likely to be stoichiometrically relevant, the Cr(III) ion incorporates as a pair of O_h coordinated Cr ions sharing an edge by removal of three Zn ions. Such an arrangement is supported by the XANES data. Charge compensation driven vacancy formation is a well-known phenomenon for metal chalcogenides, and one of the major reason p or n doping of the II−VI class is difficult to achieve.[54]

The observation of Cr(III) ion incorporation rather than as Cr(II) is interesting and is believed to reflect thermodynamic forces. Cr(III) is a d^3 metal ion which favors O_h coordination. The d^3 configuration has a lowest-lying half-filled t_{2g} orbital, inducing greater thermodynamic stability for the Cr(III) center. In fact, of the AB_2X_4 structures that are known for Cr(III) ion incorporation into II−VI semiconductor, Cr(III) shows the greatest thermodynamic potential for occupation of O_h sites.[27] Further stabilization of the center is achieved by the favorable

ionic radius of Cr(III) (0.755 Å) which can fit into O_h site formed by Zn ion vacancy, whereas Cr(II) has a much larger radius of 0.94 Å. While it might be anticipated that the formation of Cr(III) is surprising, due to better charge balance for Cr(II), observation of a change in oxidation state for a doped metal ion is observed reflecting the formation of a thermodynamically more stable oxidation for Cu(I):CdSe and Eu(III):CdSe QDs.[19,20]

While the oxidation state of the Cr ion can be rationalized, the location of the Cr(III) ions and whether it is best represented as a stochastically distributed defect in the lattice, isolated at the QD surface, or as a cluster within the QD core can only be speculated. If we assume a Poisson distribution of the Cr(III) ions, it is anticipated only localized single Cr(III) sites will form within the lattice with a 73% probability, while pair formation would be 19%, and a larger cluster would occur at 8%.[3] If we assume a cluster model, at 2.5% Cr(III) incorporation into the 2.8 nm ZnSe QD (~300 Zn ions) would generate two $n = 2$ tetrameric clusters (or four $n = 1$ dimeric clusters) from the ~8 available Cr(III) ions substituted for 12 Zn ions on average. Likewise, for a 0.4% Cr(III) doping level, this translates to only two Cr(III) centers per QD and could only produce at most a single pair of ions. The actual numbers of Cr ions will be represented as a stochastic distribution across the QDs due to the expected distribution in doping levels as the QD grows.

Incorporation of an isolated stochastic defect ion is expected to exhibit Vegard law behavior,[7] while a clustered ion or surface localized Cr(III) center is not expected to exhibit Vegard law behavior. Since XRD methods must obey Bragg's law over several lattice planes, the lack of a shift in the pXRD for the ZnCrSe QDs as a function of the doping concentration suggests that the ions are not well represented by a stochastically distributed ion producing an average lattice distortion. The alternative ion clustering model suggested by the XANES would be consistent with the lack of shift in the pXRD data.

The incorporation of Cr(III) ions as a pair into the ZnSe lattice forms the initial cell of a spinel phase of the form ACr_2X_4 (A = Cd, Zn; X = S, Se).[27] Such a structure is supported by the only available spinel phase diagram ($CdCr_2Se_4$) where a solid solution is formed for Cd to Cr ratios below 64%. In this range it is observed that a peritectoid reaction leads to the $CdCr_2Se_4$ spinel precipitating out of the metal chalcogenide crystal below 885 °C due to low solubility in the phase.[29] Inspection of the

crystal structure reveals that a spinel inclusion can be lattice matched to the cubic structure, as shown in Figure 5 by cluster
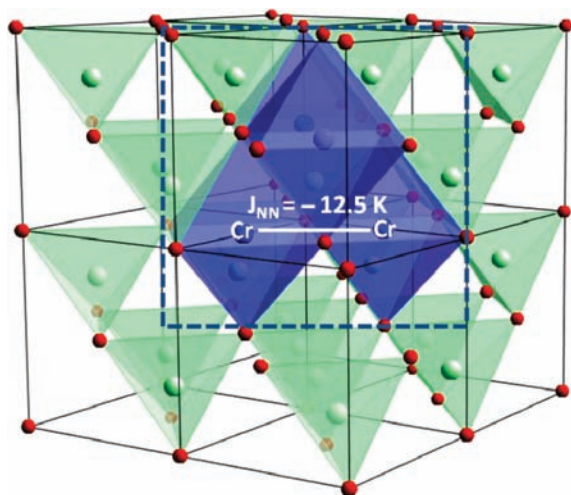

Figure 5. Illustration of the $ZnCr_2Se_4$ spinel structure composed of 4 $CrSe_6$ O_h unites embelded in the ZnSe zinc-blende lattice. The Cr(III) ions (blue balls) occupy O_h sites, and Zn(II) ions (green balls) occupy T_d sites.

precipitation as $[ZnCr_2Se_4]_n$ (n = 1, 2, ...). The structure in Figure 5 is for the n = 2 cluster produced by removal of six Zn ions at T_d sites which opens four O_h sites (six coordinate) in the lattice for incorporation of four edge-shared Cr(III) polyhedral centers. The n = 2 structure shown in Figure 5 is thermodynamically favored as the face-centered cubic (fcc) packing of Se anion of cubic phase ZnSe and $CrZn_2Se_4$ spinel provides a reasonable epitaxial match, where the group II metal occupies one-eighth of the T_d site and the Cr(III) ion occupies one-half of the octahedral (O_h) sites.[28]

The proposed model in Figure 5 is surprising and hard to prove. The size and location of a nanoscale inclusion are known to be difficult to observe by TEM or pXRD, since the inclusion is oriented along the crystallographic directions of the crystal and therefore the average structure measured by XRD is not perturbed. Since XRD requires that Bragg's law is obeyed, several lattice lanes must be present to be experimentally observable. For a single cluster within a 2.8 nm ZnSe QD, the structural imperfection will not be experimentally observable in the pXRD. TEM can provide insight, but the low Z-number and high propensity for beam damage in ZnSe limits the applicability of the technique to image the Cr(III) centers.

While TEM and pXRD provide little insight into the presence of a $ZnCr_2Se_4$ inclusion, the magnetic properties of the Cr(III) center in the $Zn_{1-x}Cr_xSe$ QD can provide insight into the cluster size, since exchange constants and the Curie temperature will reflect the number of interacting Cr centers. A $ZnCr_2Se_4$ spinel exhibits a helical spin structure as the result of competing FM and AFM interactions,[28] with a direct nearest-neighbor exchange constant of J_{NN} = −15.1 K.[30,31,55] Isolated Cr(III) centers will exhibit paramagnet behavior with insignificant exchange coupling due to the nearest-neighbor interactions dominating the exchange process. A plot of moment vs temperature should follow Curie−Weiss (C−W) law behavior. Formation of a pair of ions or larger clusters should result in high-temperature C−W behavior exhibiting AFM exchange with a nearest-neighbor exchange value (J_{NN}) calculated from the negative C−W temperature (θ, x-intercept). At low-temperature exchange coupling within a cluster will result in deviation from the C−W projection in a $ZnCr_2Se_4$ spinel inclusion due to competing FM and AFM interactions. The number of Cr(III) neighbors or cluster size can be approximated from temperature-dependent magnetic susceptibility measurements, since the exchange constant, J_{NN}/k = $3\theta/(2ZS(S + 1))$, where θ is the C−W temperature, k is the Boltzmann constant, S is the spin, and Z is the number of nearest neighbors.[7,54] The structural model presented in Figure 5 would require high-temperature C−W behavior that deviates at low T, AFM exchange (negative C−W temperature), and a J_{NN} = −15.1 K,[31] while isolated Cr(III) should result in paramagnetic (PM) behavior, $J_{NN} \sim 0$ K and $Z < 4$, depending on the Cr(III) concentration in the sample.

In Figure 6A, the ZFC and FC (200 Oe) susceptibility (χ) data for 2.5% $Zn_{1-x}Cr_xSe$ QD are shown. The experimental susceptibility and magnetization data for the $Zn_{1-x}Cr_xSe$ QDs exhibit high-temperature PM behavior as expected for the low Cr(III) content. In Figure 6A inset, the C−W law plot of the temperature-dependent data, $1/\chi = (T - \theta)*C^{-1}$ (C is the Curie constant, T is temperature in Kelvin, and θ is the C−W temperature), is shown. The C−W plot yields a negative Curie temperature (θ of −125 K) indicative of AFM exchange in the
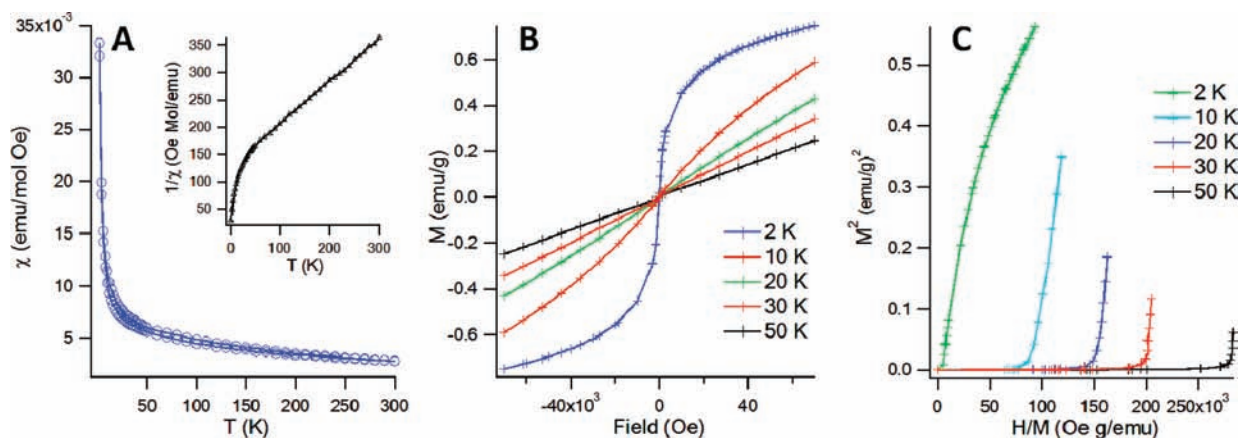

Figure 6. (A) Temperature-dependent ZFC and FC (200 Oe) susceptibility data. The insert if the C−W law plot showing negative C−W temperature (−125 K). (B) Field-dependent magnetization (M) plots at 2, 10, 20, 30, 50 K, and (C) Arrott plots (M^2 vs H/M) for the 2.5% $Zn_{1-x}Cr_xSe$ QDs.

sample, which can be accounted for by the presence of Cr(III)−Cr(III) magnetic exchange coupling between nearest-neighbor ions. The observation of exchange coupling at 2.5% Cr(II) supports a model where Cr(III) ion clustering occurs within the ZnSe QD, since it is anticipated that >73% of the ions should be isolated based on Poisson statistics. The calculated value of J_{NN} extracted from the C−W temperature θ as a function of the number of Cr(III) ions in the cluster (Z) is −25 K ($Z = 2$), −16.7 K ($Z = 3$), −12.5 K ($Z = 4$), and −10 K ($Z = 5$). The exchange coupling of ZnCr$_2$Se$_4$ with 4 Cr(III) O_h centers is close to the theoretical direct exchange constant in ZnCr$_2$Se$_4$ ($J_{NN(bulk)} = -15.1$ K). Although the poor fit for $Z = 2$ and 3 is unlikely due to the larger negative value of J_{NN}, it is worth noting that the magnetic data are easily over interpreted and cannot be used to eliminate the possibility of isolated or smaller ion clusters in the data, since a larger magnetic ion cluster will exhibit the largest observable moment particularly at high temperature, skewing the results. On the other hand if $Z = 4$ clusters were not present in the sample, then one would expect a smaller value of θ in order to obtain a J_{NN} value consistent with bulk structures for $Z < 4$.

The assignment of a PM behavior with AFM exchange coupling is confirmed by field-dependent magnetization (M) plots for 2.5% Zn$_{1-x}$Cr$_x$Se (Figure 6B). The magnetization data at 2 K show saturation above 2 T but exhibit no hysteresis at all measured temperatures. The absence of FM order in the 2.5% Zn$_{1-x}$Cr$_x$Se QDs can be verified by plotting the field-dependent data as Arrott plots in Figure 6C (M^2 vs H/M at fixed temperatures). In the Arrott plots, the Curie temperature (T_c) for ferromagnetism is determined from the temperature, where M^2 intercepts with the origin.[56] The Arrott plots show a linear H/M dependence from 10−50 K. Consistent with a PM material, in the Arrott plot M^2 approaches a value of zero as the $T \to 0$ K. The data at 2 K exhibits curvature in the Arrott plot which can be interpreted in analogy to the Arrott plot in bulk materials where competing magnetic exchange interactions exist at low temperature.[57] The competing magnetic behavior supports the spinel inclusion model within the QD lattice, since the competition between FM and AFM interactions in bulk ZnCr$_2$Se$_4$ spinel results in an overall helical spin state.

The magnetic data, and particularly the agreement in the J_{NN} values between bulk ZnCr$_2$Se$_4$ and the $Z = 4$ calculation, are in support of the proposed structure in Figure 5, where the formation of four edge-shared Cr(III) O_h centers in the ZnSe lattice gives rise to short-range Cr(III)−Cr(III) magnetic exchange. Coupled with the likelihood that a peritectoid reaction requires a critical nuclei to form in order to precipitate, a $n = 2$ or larger cluster is reasonable for a proposed structural motif and is supported by the magnetic, XANES, HF-EPR, and optical data by comparison to bulk spinel values and is consistent with the observation of no significant structural distortion occurring in the metal and chalcogenide sublattices, since the Zn and Se L$_3$ edge XANES data are not strongly affected compared to the energies observed in bulk spinel structures (Figure SF6, Supporting Information).[58] More importantly the defect clustering model within a QD is reported in the literature and supported by the phase diagrams for Cr(III) incorporation into a metal chalcogenide lattice.

Site Occupation of Cr(III) Ions. Although the XANES, absorption spectra, HF-EPR, and the magnetic data support a Cr(III) spinel inclusion in the ZnSe QD, the experimental data cannot distinguish between precipitation at the QD surface from incorporation into the QD. In anlogy to experimental

interrogation of the structural motif in CdSSe alloys and a CdMnSe alloys in a previous series of reports,[59,60] chemical etching experiements can provide some insight into the location of the Cr ion cluster by analyzing a spectroscopic signature for Cr following removal of the outermost shells from the circumference of the QD. If we consider a 2.8 nm diameter 2.5% Zn$_{1-x}$Cr$_x$Se QD, which consists of 10 ZnSe planes (5 shells) projected along the ⟨111⟩ direction, etching to remove ∼1 shell results in a reduction of the QD diameter by 0.6 nm, generating a ∼2.2 nm QD. The 2.2 nm QD is composed of ∼7 planes projected along the ⟨111⟩ crystallographic direction or ∼3−4 shells. The 2.2 nm QD has ∼120 ions forming the Zn sublattice. For a Cr(III) species isolated at the QD surface, one would expect a complete loss of the spectroscopic signature for Cr ions if the cluster is isolated either in the outermost shells of the QD or as a phase segregated surface species after the sample was isolated from the etching solution. On the other hand incorporation into the QD core should not impact the presence of Cr in the QD after etching. For the statement to be valid, the chemcial etching study requires that the rate of etching of the ZnSe and the ZnCr$_2$Se$_4$ spinel is similar.

Surface etching of the ZnSe QD was carried out using 20 μL H$_3$PO$_4$:HCl (1:1 V:V) in 1 mL saturated toluene solution.[59,61] The QD samples were etched for 2 s at room temperature, which shifts the 1S$_{3/2}$ → 1S$_e$ first exciton peak shift from 375 to 257 nm (Figure SF7, Supporting Information). The shift in the first exciton is consistent with the removal of ∼0.8 nm from the QD surface or ∼1−2 shells from the circumference of the QD. The etched samples were precipitated by the addition of MeOH, redissolved in toluene, and reprecipitated by MeOH prior to conducting the EPR experiments. Although the QD was etched by ∼0.8 nm, the resultant EPR spectra following chemical etching produce no change to the EPR (Figure SF7, Supporting Information) spectral manifold, indicating the Cr(III) ions are within the QD and not isolated at the surface of the QD.

The lack of a spectral change to the EPR is indicative of the Cr spinel inclusion forming within the ZnSe QD. It is expected that if the Cr ion cluster is within the core of the QD that the Cr concentration must increase from 2.5% in a 2.8 nm Zn$_{1-x}$Cr$_x$Se QD to a value between 6−9% in a 2.0 nm QD to account for the change in Zn to Cr ratio as the QD is etched. Analysis of the XRF data following etching indicates the Cr content increases from 2.5 to 8 mol % relative to the Zn ion, confirming the theoretical prediction (Table 2, Supporting Information). The facts the Cr(III) ion is still evident in the EPR and the Cr content increases with decreasing QD size are strong confirmation that the ZnCr$_2$Se$_4$ inclusion occupies a core site within the 2.0 nm QD.

CONCLUSION

While in bulk reactions the formation of MCr$_2$X$_4$ spinels as a single phase or as inclusions in the MX lattice are observed to be formed by reaction of the metal chalcogenide via a a peritectoid reaction, the structural motif has not been reported for QDs. Whether the core inclusion reflects initial nucleation in the spinel phase followed by growth of the ZnSe shell or occurs due to similar kinetic rates of ion addition is not clear. The incorporation of a Cr(III) ion on a tetragonally distorted O_h site is proven by the Cr L$_{2,3}$ edge XANES spectra. The absorption spectra for the Zn$_{1-x}$Cr$_x$Se QDs confirm the oxidation state assigned and allow the crystal field energy to be calculated (10 Dq = 2.08 eV) from the $^4A_{2g} \to {}^4T_{2g}$ crystal

field transition. The nearly identical value for 10Dq from absorption and the simulated XANES data indicates the Cr(III) ion is tetragonally distorted due to pair formation of Cr octahedral by removal of three Zn ions for each pair of Cr ions in the lattice. The sharing of the O_h edge by the Cr(III) ions in the ZnSe lattice produces a minimally distorted site in the lattice analogous to spinel inclusions in bulk metal chalcogenide structures. The ZFC/FC susceptibility measurement shows PM behavior with AFM exchange coupling at low temperature. The calculated Cr(III)−Cr(III) J_{NN} value ($Z = 4$) for the QD (−12.5 K) is consistent with reported bulk values and supports a model of $ZnCr_2Se_4$ spinel inclusion within the core of the QD. High-frequency EPR data are quite consistent with Cr (III) in an O_h environment, exhibiting only the Zeeman interaction and no other splitting. Further studies are underway to analyze the Cr−Cr nearest-neighbor distances via EXAFS and the exchange coupling of the inclusion to the band structure of the ZnSe lattice using XMCD and magneto-optical methods. The intriguing ability to incorporate a magnetic inclusion in an otherwise crystalline QD opens a new class of dilute magnetic semiconductor QDs for further studies.

■ ASSOCIATED CONTENT

Ⓢ Supporting Information

TEM images and size disperisty analysis, UV−vis and Cr(III) concentration-dependent PL quantum yield, XRF elemental composition, pXRD comparisons to standards, crystal field spectra fit of the $^4A_{2g} \rightarrow {}^4T_{2g}$ transition, theoretical splitting behavior for Cr(III) EPR, Zn and Se L_3 edge XANES data, and EPR and XRF data after chemical etching of 2.5% $Zn_{1-x}Cr_xSe$ QDs. This material is available free of charge via the Internet at http://pubs.acs.org.

■ AUTHOR INFORMATION

Corresponding Author

strouse@chem.fsu.edu

Notes

The authors declare no competing financial interest.

■ ACKNOWLEDGMENTS

■ REFERENCES

(1) Erwin, S. C.; Zu, L. J.; Haftel, M. I.; Efros, A. L.; Kennedy, T. A.; Norris, D. J. *Nature* **2005**, *436*, 91−94.

(2) Norris, D. J.; Efros, A. L.; Erwin, S. C. *Science* **2008**, *319*, 1776−1779.

(3) Bryan, J. D.; Gamelin, D. R. In *Progress in Inorganic Chemistry*; Karlin, K. D., Ed.; John Wiley & Sons, Inc.: Hoboken, NJ, 2005; Vol. 54, pp 47−126.

(4) Norris, D. J.; Yao, N.; Charnock, F. T.; Kennedy, T. A. *Nano Lett.* **2001**, *1*, 3−7.

(5) Beaulac, R.; Archer, P. I.; Ochsenbein, S. T.; Gamelin, D. R. *Adv. Funct. Mater.* **2008**, *18*, 3873−3891.

(6) Yu, J. H.; Liu, X.; Kweon, K. E.; Joo, J.; Park, J.; Ko, K.-T.; Lee, D. W.; Shen, S.; Tivakornsasithorn, K.; Son, J. S.; Park, J.-H.; Kim, Y.-W.; Hwang, G. S.; Dobrowolska, M.; Furdyna, J. K.; Hyeon, T. *Nat. Mater.* **2010**, *9*, 47−53.

(7) Hanif, K. M.; Meulenberg, R. W.; Strouse, G. F. *J. Am. Chem. Soc.* **2002**, *124*, 11495−11502.

(8) Pradhan, N.; Peng, X. *J. Am. Chem. Soc.* **2007**, *129*, 3339−3347.

(9) Mikulec, F. V.; Kuno, M.; Bennati, M.; Hall, D. A.; Griffin, R. G.; Bawendi, M. G. *J. Am. Chem. Soc.* **2000**, *122*, 2532−2540.

(10) Wolf, S. A.; Awschalom, D. D.; Buhrman, R. A.; Daughton, J. M.; von Molnár, S.; Roukes, M. L.; Chtchelkanova, A. Y.; Treger, D. M. *Science* **2001**, *294*, 1488−1495.

(11) Ohno, H. *Science* **1998**, *281*, 951−956.

(12) Dietl, T. *Nat. Mater.* **2010**, *9*, 965−974.

(13) Meulenberg, R. W.; Lee, J. R. I.; McCall, S. K.; Hanif, K. M.; Haskel, D.; Lang, J. C.; Terminello, L. J.; van Buuren, T. *J. Am. Chem. Soc.* **2009**, *131*, 6888−6889.

(14) Neeleshwar, S.; Chen, C. L.; Tsai, C. B.; Chen, Y. Y.; Chen, C. C.; Shyu, S. G.; Seehra, M. S. *Phys. Rev. B* **2005**, *71*, 201307.

(15) Zheng, W.; Strouse, G. F. *J. Am. Chem. Soc.* **2011**, *133*, 7482−7489.

(16) Norman, T. J.; Magana, D.; Wilson, T.; Burns, C.; Zhang, J. Z.; Cao, D.; Bridges, F. *J. Phys. Chem. B* **2003**, *107*, 6309−6317.

(17) Archer, P. I.; Santangelo, S. A.; Gamelin, D. R. *Nano Lett.* **2007**, *7*, 1037−1043.

(18) Zheng, W.; Kumar, P.; Washington, A.; Wang, Z.; Dalal, N. S.; Strouse, G. F.; Singh, K. *J. Am. Chem. Soc.* **2012**, *134*, 2172−2179.

(19) Meulenberg, R. W.; van Buuren, T.; Hanif, K. M.; Willey, T. M.; Strouse, G. F.; Terminello, L. J. *Nano Lett.* **2004**, *4*, 2277−2285.

(20) Raola, O. E.; Strouse, G. F. *Nano Lett.* **2002**, *2*, 1443−1447.

(21) Title, R. S. *Phys. Rev.* **1964**, *133*, A1613.

(22) Estle, T. L.; Holton, W. C. *Phys. Rev.* **1966**, *150*, 159.

(23) Boonman, M. E. J.; Mac, W.; Twardowski, A.; Wittlin, A.; van Bentum, P. J. M.; Maan, J. C.; Demianiuk, M. *Phys. Rev. B* **2000**, *61*, 5358.

(24) Vallin, J. T.; Watkins, G. D. *Phys. Rev. B* **1974**, *9*, 2051.

(25) Rai, R.; Savard, J. Y.; Tousignant, B. *Phys. Lett. A* **1967**, *25*, 443−444.

(26) Stefaniuk, L.; Bester, M.; Virt, I. S.; Kuzma, M. *Acta Phys. Pol., A* **2005**, *108*, 413−418.

(27) Henning, V. P. *J. Cryst. Growth* **1971**, *9*, 296−304.

(28) Ohgushi, K.; Okimoto, Y.; Ogasawara, T.; Miyasaka, S.; Tokura, Y. *J. Phys. Soc. Jpn.* **2008**, *77*, 034713.

(29) Barraclough, K. G.; Meyer, A. *J. Cryst. Growth* **1973**, *20*, 212−216.

(30) Menyuk, N.; Dwight, K.; Arnott, R. J.; Wold, A. *J. Appl. Phys.* **1966**, *37*, 1387−1388.

(31) Siratori, K. *J. Phys. Soc. Jpn.* **1971**, *30*, 709−719.

(32) Akimitsu, J.; Siratori, K.; Shirane, G.; Iizumi, M.; Watanabe, T. *J. Phys. Soc. Jpn.* **1978**, *44*, 172−180.

(33) Hemberger, J.; von Nidda, H. A. K.; Tsurkan, V.; Loidl, A. *Phys. Rev. Lett.* **2007**, *98*, 147203.

(34) Murakawa, H.; Onose, Y.; Ohgushi, K.; Ishiwata, S.; Tokura, Y. *J. Phys. Soc. Jpn.* **2008**, *77*, 043703.

(35) Siratori, K.; Kita, E. *J. Phys. Soc. Jpn.* **1980**, *48*, 1443−1448.

(36) Kalinnikov, V. T.; Aminov, T. G.; Novotortsev, V. M. *Inorg. Mater.* **2003**, *39*, 997−1012.

(37) Lamonova, K.; Ivanchenko, I.; Orel, S.; Paranchich, S.; Tkach, V.; Zhitlukhina, E.; Popenko, N.; Pashkevich, Y. *J. Phys.: Condens. Matter* **2009**, *21*.

(38) Quarez, E.; Hsu, K.-F.; Pcionek, R.; Frangis, N.; Polychroniadis, E. K.; Kanatzidis, M. G. *J. Am. Chem. Soc.* **2005**, *127*, 9177−9190.

(39) Cumberland, S. L.; Hanif, K. M.; Javier, A.; Khitrov, G. A.; Strouse, G. F.; Woessner, S. M.; Yun, C. S. *Chem. Mater.* **2002**, *14*, 1576−1584.

(40) Magana, D.; Perera, S. C.; Harter, A. G.; Dalal, N. S.; Strouse, G. F. *J. Am. Chem. Soc.* **2006**, *128*, 2931−2939.

(41) Lovingood, D. D.; Achey, R.; Paravastu, A. K.; Strouse, G. F. *J. Am. Chem. Soc.* **2010**, *132*, 3344−3354.

(42) Cage, B.; Hassan, A. K.; Pardi, L.; Krzystek, J.; Brunel, L.-C.; Dalal, N. S. *J. Magn. Reson.* **1997**, *124*, 495−498.

(43) van Tol, J.; Brunel, L. C.; Wylde, R. J. *Rev. Sci. Instrum.* **2005**, *76*, 074101.

(44) Morley, G. W.; Brunel, L. C.; van Tol, J. *Rev. Sci. Instrum.* **2008**, *79*, 064703.

(45) Regier, T.; Paulsen, J.; Wright, G.; Coulthard, I.; Tan, K.; Sham, T. K.; Blyth, R. I. R. In *9th International Conference on Synchrotron Radiation Instrumentation*; Springer: New York, **2007**; Vol. *879*, p 473−476.

(46) Stavitski, E.; de Groot, F. M. F. *Micron* **2010**, *41*, 687−694.

(47) Rudolf, T.; Kant, C.; Mayr, F.; Schmidt, M.; Tsurkan, V.; Deisenhofer, J.; Loidl, A. *Eur. Phys. J. B* **2009**, *68*, 153−160.

(48) Farvid, S. S.; Ju, L.; Worden, M.; Radovanovic, P. V. *J. Phys. Chem. C* **2008**, *112*, 17755−17759.

(49) Thorp, J. S.; Skinner, A. R.; Al-Hawery, A. S. *J. Magn. Magn. Mater.* **1989**, *81*, 47−55.

(50) Krzystek, J.; Ozarowski, A.; Telser, J. *Coord. Chem. Rev.* **2006**, *250*, 2308−2324.

(51) Carlin, R. L. *Magnetochemistry*; Springer-Verlag: Berlin, Germany, 1985.

(52) VanMil, B. L.; Ptak, A. J.; Bai, L.; Wang, L. J.; Chirila, M.; Giles, N. C.; Myers, T. H.; Wang, L. *J. Electron. Mater.* **2002**, *31*, 770−775.

(53) Estle, T. L.; Holton, W. C. *Phys. Rev.* **1966**, *150*, 159−167.

(54) Furdyna, J. K. *J. Appl. Phys.* **1988**, *64*, R29−R64.

(55) Baltzer, P. K.; Wojtowicz, P. J.; Robbins, M.; Lopatin, E. *Phys. Rev.* **1966**, *151*, 367−377.

(56) Arrott, A. *Phys. Rev.* **1957**, *108*, 1394−1396.

(57) Yeung, I.; Roshko, R. M.; Williams, G. *Phys. Rev. B* **1986**, *34*, 3456−3457.

(58) Zimnal-Stamawska, M.; Czarnecka-Such, E.; Kisiel, A.; Frentrup, W.; Giriat, W. *J. Phys. IV* **1997**, *7*, 1201−1202.

(59) Lovingood, D. D.; Oyler, R. E.; Strouse, G. F. *J. Am. Chem. Soc.* **2008**, *130*, 17004−17011.

(60) Zheng, W.; Wang, Z.; Wright, J.; Goundie, B.; Dalal, N. S.; Meulenberg, R. W.; Strouse, G. F. *J. Phys. Chem. C* **2011**, *115*, 23305−23314.

(61) Wosten, W. J. *J. Appl. Phys.* **1962**, *33*, 246−247.